Preparation and Characterization of Novel Organic/Inorganic Hybrid Nanoparticles Containing an Organotin Core and a Polystyrene Shell

Yong-Guang Jia, Jian Jiang, Ling-Yan Liu, Wei-Xing Chang, Jing Li

State Key Laboratory of Elemento-Organic Chemistry, The department of Chemistry, Nankai University, Tianjin 300071, People's Republic of China

Received 5 May 2011; accepted 8 November 2011
DOI 10.1002/app.36467
Published online in Wiley Online Library (wileyonlinelibrary.com).

ABSTRACT: A series of new well-defined nanoparticles containing an organotin core and a polystyrene shell were obtained by crosslinking of *n*-Bu_2SnO with various chain-length amphiphilic polystyrene-*b*-poly-(6-(4-vinylphenoxy) hexanoic acid. The amphiphilic copolymers were synthesized via reversible addition fragmentation chain transfer polymerization and hydrolysis. The structures of the nanoparticles were studied by the transmission electron microscopy, scanning electron microscopy, and X-ray photoelectron spectroscopy analysis. Notably, the morphology of the crosslinked copolymer showed individual nanoparticles with regularly spherical shape. And the nanoparticle diameters decreased with increasing number of organotin carboxylate units. © 2012 Wiley Periodicals, Inc. J Appl Polym Sci 000: 000–000, 2012

Key words: organotin; nanoparticles; core-shell; crosslink; RAFT

INTRODUCTION

Block copolymers have attracted increasing attention due to their ability to readily form organized micellar aggregates with well-defined nanoscopic morphologies.[1,2] Furthermore, the versatile nanostructures constructed by self-assembly of block copolymers have been widely applied in nanotechnologies.[3–7] With the development of controlled/living radical polymerization techniques, various functional groups have been incorporated into block copolymer structures.[8–11] In addition, it has long been recognized that introducing metal atoms into the one-dimensional chains of polymers may result in desirable physical and chemical properties.[12–15] Based on this concept, various approaches and techniques have been successfully developed to prepare metal-containing polymers during the past several decades.[16] Among these approaches, the combination of a reactive amphiphilic diblock copolymer with organometallic compounds is an important method to obtain metal-containing polymers. For example, Chen and coworkers[17–20] has synthesized various organic/inorganic nanomaterials based on the sol-gel process of alkoxylsilyl groups.

However, to the best of our knowledge, few report focused on the design, preparation, and morphology of organotin-containing block copolymers.[21–30] Organotin compounds, as the most intensively studied species,[31,32] are more stable than most of other organometallic compounds, because tin is in the same group as carbon. And these organotin compounds possess considerable structural diversity and topologies[33,34] (e.g., monomers, dimers, tetramers, oligomeric ladders, and hexameric drums).[35] Moreover, their applications cover a wide range of different fields, such as antifouling paints,[36] polyvinylchloride stabilizers,[37] and antitumor drugs,[38] as well as anion carriers in electrochemical membrane designs[39] and homogeneous catalysts.[40] To date, most organotin-containing copolymers are based on triorganotin carboxylates, and they are synthesized by esterification of carboxylic groups with bis(tributyltin) oxide or direct polymerization of triorganotin carboxylate monomers.[21–24] The triorganotin-containing copolymers are lower catalytic activity and less functional compared with diorganotin compounds due to the less versatile structural diversity and topologies, though they are easily prepared. Nevertheless, there are few reports concerning diorganotin-containing polymers, as the controlled synthesis of these polymers being relatively difficult.

Additional Supporting Information may be found in the online version of this article.

Correspondence to: L.-Y. Liu (liulingyan@nankai.edu.cn) or J. Li (lijing@nankai.edu.cn).

Contract grant sponsor: National Natural Science Foundation of China; contract grant number: 21072099.

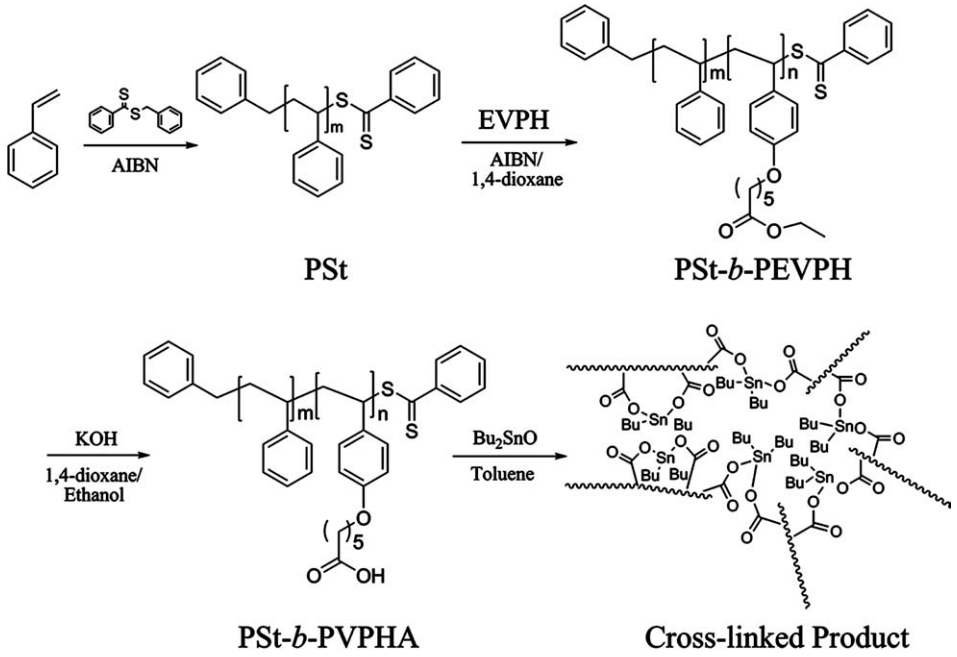

Scheme 1 Procedure for the preparation of nanoparticles.

With this in mind, a series of new diorganotin-containing copolymers were designed and synthesized by the use of crosslinking between *n*-Bu_2SnO and polystyrene-*b*-poly (6-(4-vinylphenoxy)hexanoic acid) (**PSt-*b*-PVPHA**) (Scheme 1). A pentamethylenic spacer between carboxyl acid and backbone was added in the *para*-position of the phenyl ring of styrene. This spacer can provide a sufficiently long distance for the complete crosslinking between **VPHA** units and *n*-Bu_2SnO. Furthermore, we mainly focused on the investigation of the relationship between the morphology and the structure of the block copolymer.

EXPERIMENTAL

Materials

Styrene was purchased from Acros (99%), purified by filtration through alumina (to remove inhibitors), stirred with CaH_2 overnight at room temperature, and distilled under reduced pressure before use. 1,1′-Azobis(isobutironitrile) (AIBN) (>98%, the Sixth Reagent Factor of Tianjin) was recrystallized twice from methanol. Benzyl benzodithioate and ethyl 6-(4-vinylphenoxy) hexanoate (EVPH) were synthesized according to the literature, respectively.[41,42] Potassium hydroxide, *n*-Bu_2SnO, potassium carbonate, bromomethylbenzene, bromobenzene, carbon disulfide, and magnesium were purchased from the Sixth Reagent Factor of Tianjin and were used as received. All other common solvents were purified using standard procedures.

Characterizations

^{1}H-NMR and ^{13}C-NMR spectra were recorded on a Varian Mercury 400 MHz spectrometer at room temperature, with tetramethylsilane as an internal standard. Molecular weights and molecular weight distributions were measured on a Waters Gel Permeation Chromatography (GPC) [Waters 1515 liquid chromatography connected with three Waters styragel GPC columns (HT2, HT3, and HT4) and a Waters 2414 refractive index detector; eluent, tetrahydrofuran (THF); flow rate, 1 mL min^{-1}; temperature, 40°C]. The instrument was calibrated with monodispersed polystyrenes as standards. Fourier Transform-Infrared (FTIR) spectra were recorded using KBr pellets for solid samples on a Bruker EQUINOX 55. Scanning electron microscopy (SEM) images were obtained using a SHIMADZU ss-550 instrument. Samples (0.5 mg mL^{-1} in THF) were dropped onto glass sheets and sputter-coated with gold. The particle diameter was measured by counting and measuring at least 100 particles in the SEM images. Transmission electron microscopy (TEM) images were analyzed using a Tecnai G2 20 S-TWIN electron microscopy equipped with a Model 794 CCD camera (512 × 512) (gatan) with an accelerating voltage of 200 kV. Sample (0.5 mg mL^{-1} in THF) solutions were dropped onto 300 mesh copper TEM grids and dried for 7 days at room temperature. X-ray photoelectron spectroscopy (XPS) was recorded using a Kratos Axis Ultra delay line detector (DLD) spectrometer using a monochromated Al-Ka X-ray

source (hv = 1486.6 eV), hybrid (magnetic/electrostatic) optics, and a multichannel plate and DLD. All XPS spectra were recorded using an aperture slot of 300 × 700 μm^2, survey spectra with a pass energy of 160 eV, and high resolution spectra with a pass energy of 40 eV. Elemental analysis was performed on a Chncorder-MF-3. Dynamic light scattering (DLS) measurements were performed on a laser light scattering spectrometer (BI-200SM) equipped with a digital correlator (BI-10000AT) at 532 nm. Filtering solutions (1 mL) through a 0.45 μm Millipore filter into a clean scintillation vial was manipulated to obtain the samples, and the characterization was operated at 25°C.

Synthesis of EVPH

A mixture of methyltriphenylphosphonium iodide (7.350 g, 18.19 mmol), K_2CO_3 (2.740 g, 19.85 mmol), and tetrabutylammonium bromide (0.531 g, 1.65 mmol) was added to a dry 250 mL round-bottom flask under nitrogen atmosphere. The flask was subsequently degassed and purged with nitrogen three times. Then, 60 mL 1,4-dioxane was added to flask under nitrogen, followed by refluxing for 1 h while stirring. Ethyl 6-(4-formylphenoxy) hexanoate (4.102 g, 16.54 mmol)[43] dissolved in 30 mL 1,4-dioxane and was added to the flask, and refluxing was continued until the ethyl 6-(4-formyl-phenoxy) hexanoate disappeared. The mixture was filtered to remove the solids, and filtrate was concentrated to yield a yellow liquid. The crude residue was isolated by chromatography on a silica gel column using 1 : 20/v : v ethyl acetate : petroleum ether as an eluent to yield 3.511 g colorless liquid. Yield: 81%. ^{1}H-NMR ($CDCl_3$, ppm): δ 7.33 (d, 2H), 6.84 (d, 2H), 6.65 (dd, 1H), 5.60 (dd, 1H), 5.11 (dd, 1H), 4.13 (q, 2H), 3.96 (t, 2H), 2.33 (t, 2H), 1.80 (m, 2H), 1.70 (m, 2H), 1.50 (m, 2H),1.26 (t, 3H), ^{13}C-NMR ($CDCl_3$, ppm): δ 173.3 (1C), 158.9 (1C), 136.3 (1C), 130.2 (1C),127.3 (2C), 114.4 (2C), 111.2 (1C), 67.6 (1C), 60.1 (1C), 34.1 (1C) ,28.9 (1C), 25.6 (1C), 24.7 (1C), 14.2 (1C). Anal. Calcd for $C_{16}H_{22}O_3$: C, 73.25; H, 8.45. Found: C, 73.24; H, 8.25.

Polymerization of styrene via reversible addition fragmentation chain transfer polymerization (PSt)

In a typical reaction, benzyl benzodithioate (43.0 mg, 0.176 mmol) and AIBN (9.0 mg, 0.071 mmol) were added to a dry 50 mL Schlenk flask equipped with a stirring bar under nitrogen atmosphere. The flask was degassed and purged with nitrogen for 1 h. Styrene (5.454 g, 52.37 mmol) was added to the flask under nitrogen. Next, the tube was sealed with a septum, and residual oxygen in the mixture was removed by three freeze-pump-thaw cycles. The reaction mixture was allowed to thaw and was immersed in a preheated oil bath at 60°C for 44 h. The tube was placed into ice water to quench the reaction. The conversion of styrene was determined by ^{1}H-NMR to be 66.3%. The reaction mixture was diluted with 5 mL THF and was precipitated into excess methanol. The precipitate was washed several times with methanol and dried under vacuum to give 3.045 g of **PSt** as a pink powder.

Synthesis of polystyrene-*b*-poly(ethyl 6-(4-vinylphenoxy) hexanoate) (PSt_{196}-*b*-$PEVPH_{51}$)

PSt_{196} (437.0 mg, 0.0211 mmol), AIBN (2.0 mg, 0.0122 mmol), and **EVPH** (1.043 g, 3.981 mmol) were added to a dry 50 mL Schlenk flask equipped with a stirring bar under nitrogen atmosphere. The flask was degassed and purged with nitrogen for 1 h, and then 4 mL 1,4-dioxane was added to the flask. Next, the tube was sealed with a septum, and residual oxygen in the mixture was removed by three freeze-pump-thaw cycles. The reaction mixture was allowed to thaw and was immersed in a preheated oil bath at 60°C for 48 h. The flask was placed into ice water to quench the reaction, and the conversion of **EVPH** was determined by ^{1}H-NMR to be 28.4%. The reaction mixture was precipitated in excess methanol. The precipitate was washed several times with excess methanol and dried under vacuum to give 0.674 g of **PSt_{196}-*b*-$PEVPH_{51}$** as a white powder.

Synthesis of polystyrene-*b*-poly (6-(4-vinylphenoxy) hexanoic acid) (PSt_{196}-*b*-$PVPHA_{51}$)

A mixture of **PSt_{196}-*b*-$PEVPH_{51}$** (300.0 mg, 0.0088 mmol) and KOH (50.0 mg, 0.893 mmol) dissolved in 40 mL 1,4-dioxane and 20 mL ethanol and was stirred at 60°C for 24 h. The resulting mixture was concentrated, diluted with 50 mL distilled water, and acidified by dropping 0.5 mL concentrated hydrochloric acid followed by stirring for 2 h. The reaction mixture was filtered, washed with excess distilled water, and dried under vacuum to yield 263.0 mg of **PSt_{196}-*b*-$PVPHA_{51}$** as a white powder.

Preparation of polystyrene-*b*-poly(dibutylstannanediyl bis(6-(4-vinylphenoxy) hexanoate)) (crosslinked product)

A mixture of **PSt_{196}-*b*-$PVPHA_{51}$** (142.0 mg, 0.0044 mmol) and n-Bu_2SnO (26.0 mg, 0.104 mmol) was refluxed in 30 mL toluene for 12 h. The resulting mixture was filtered, concentrated to 1 mL, added to 50 mL methanol, filtered, and dried under vacuum to yield 154 mg of crosslinked product **C** as the white solid.

TABLE I
Characteristics of PSt and PSt-*b*-PEVPH

(Co)polymer sample	Conv. (%)[a]	$M_{n,\text{theor}}$ (10^3)[b]	$M_{n,\text{GPC}}$ (10^3)[c]	M_w/M_n[c]
PSt_{196}	66.3	20.6	21.2	1.13
PSt_{203}	68.6	21.2	24.4	1.20
PSt_{203}-*b*-$PEVPH_{13}$	9.1	24.9	25.3	1.26
PSt_{196}-*b*-$PEVPH_{34}$	19.4	29.6	26.9	1.24
PSt_{196}-*b*-$PEVPH_{51}$	28.4	34.0	33.1	1.28
PSt_{196}-*b*-$PEVPH_{103}$	40.3	47.6	47.3	1.32

[a] Conversion was calculated by ^{1}H-NMR.
[b] $M_{n,\text{theor}} = [M]_0/[\text{RAFT}]_0^* \times$ conversion %* molecular weight (M_w) of monomer + M_w of RAFT.
[c] Determined by GPC (in THF, PS standard).

RESULTS AND DISCUSSION

Synthesis and characterization of PSt and PSt-*b*-PEVPH

Two different chain length polystyrenes (**PSts**) were prepared via reversible addition fragmentation chain transfer polymerization (RAFT) in different initial molar ratios of styrene and benzyl benzodithioate. These **PSts** macroinitiators reinitiated **EVPH** at 60°C in 1,4-dioxane under the same conditions and four new diblock copolymers (**PSt-*b*-PEVPH**) with different units of **EVPH** were obtained. In Table I, we could found that the GPC-determined $M_{n,\text{GPC}}$ were closer to the theoretical molecular weight ($M_{n,\text{th}}$), and the polydispersities were all narrow (<1.32). Additionally, the analysis of GPC before and after initiation of the **EVPH** (Supporting Information Fig. S1) revealed a shift toward higher molar masses that were in agreement with the formation of the **PSt-*b*-PEVPH** diblock copolymer. Moreover, no trace of residual macroinitiator was detected by GPC. It indicates that nearly all **PSt** chains were involved in the initiation of **EVPH**. From the ^{1}H-NMR spectra (Fig. 1), the resonance peaks of two blocks were clearly assigned. In the IR spectrum, a new strong absorption peak of the ester carbonyl group in the **EVPH** units occurred at 1733 cm^{-1}, and the peak intensity increased with increasing numbers of **EVPH** units in each copolymer (Fig. 2). All the above results suggested that the RAFT polymerization was successful. In addition, the numbers of **PSt** and **EVPH** units in each copolymer were calculated by the relative integration ratio in the ^{1}H-NMR spectra.

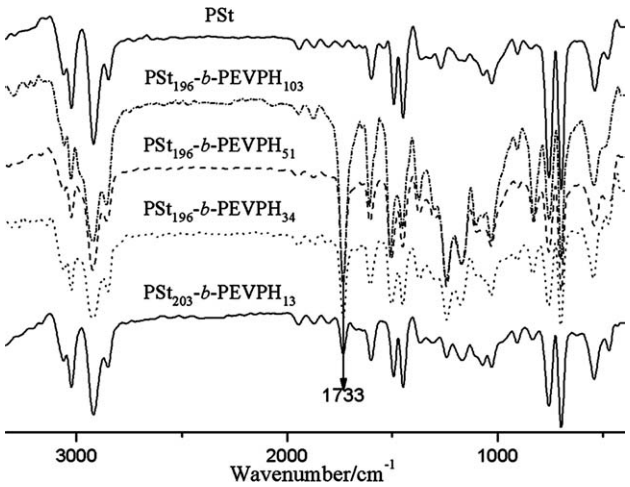

Figure 2 FTIR spectra of PSt and PSt-*b*-PEVPH.

Synthesis and characterization of PSt-*b*-PVPHA

VPHA units were synthesized by the treatment of **PSt-*b*-PEVPH** with KOH in mixture solvents of 1,4-dioxane and ethanol. This hydrolysis reaction was monitored by ^{1}H-NMR spectroscopy until the disappearance of the signal of the ethoxy protons at $\delta = 4.1$ ppm (Fig. 3). All the signals of the **PSt-*b*-PVPHA** were observable in a mixture of $CDCl_3$ and

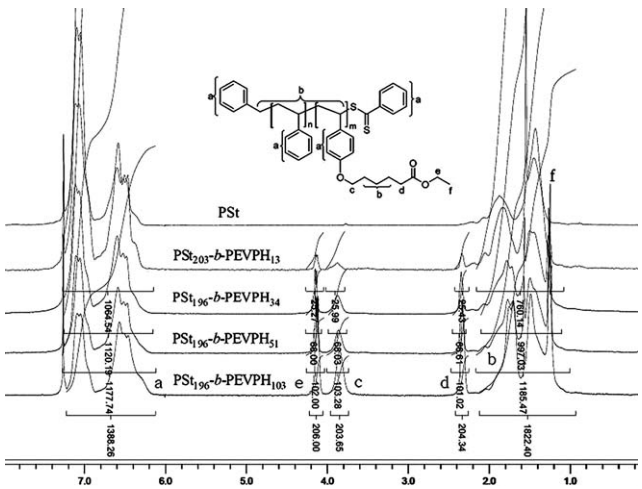

Figure 1 ^{1}H-NMR spectra of **PSt** and **PSt-*b*-PEVPH** in $CDCl_3$.

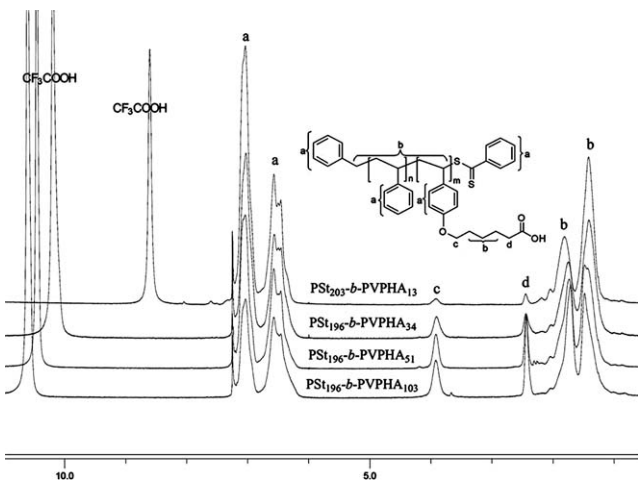

Figure 3 ^{1}H-NMR spectra of **PSt-*b*-PVPHA** taken in mixture of $CDCl_3/CF_3COOH$ (25 : 1, v/v).

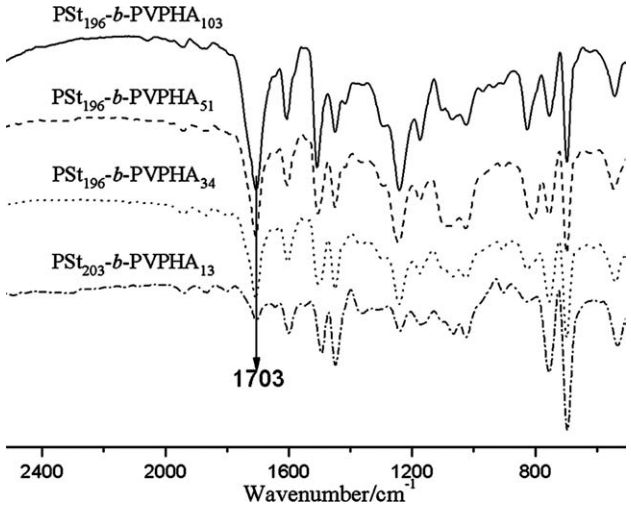

Figure 4 FTIR spectra of PSt-*b*-PVPHA.

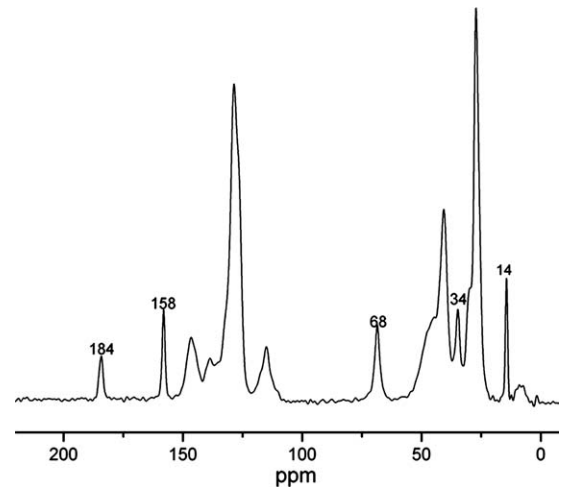

Figure 6 Solid-state ^{13}C-NMR of crosslinked product D.

CF_3COOH. Additionally, the IR spectra showed a new peak at 1703 cm^{-1} assigned to the acid carbonyl in **VPHA** units (Fig. 4), which was greatly different from the ester carbonyl (1733 cm^{-1}) in **EVPH** units. These NMR and IR results strongly suggested the complete hydrolysis of the EPVH units.

Preparation and characterization of crosslinked products

A crosslinking esterification of **VPHA** units with *n*-Bu_2SnO (Scheme 1) was designed to obtain organotin-containing nanoparticles. As a result, the reaction between **VPHA** units and *n*-Bu_2SnO easily occurred in toluene under refluxing. The corresponding crosslinked product dissolved poorly in dimethyl sulfoxide (DMSO) or $CDCl_3$, and just the signal of block **PSt** was found in the ^{1}H-NMR spectrum in $CDCl_3$ (Fig. 5). In principle, there are only two possibilities for this phenomenon: (a) there was only one block in polymer (i.e., the other was lost in the reaction); or (b) there were indeed two copolymer blocks but one surrounded by the other, leading to the disappearance of the second signal in the ^{1}H-NMR spectra. The crosslinked products did not completely dissolve in $CDCl_3$ maybe indicate another block still exists.

To determine the components of the crosslinked product, we analyzed the solid-state ^{13}C-NMR spectra of the crosslinked product between **PSt$_{196}$-*b*-PVPHA$_{103}$** and *n*-Bu_2SnO (Fig. 6). The peak of aromatic ring carbon directly connected to the oxygen atom appeared at 158 ppm. Furthermore, the chemical shifts of the alkyl carbon connected to an oxygen atom and a C=O carbon were observed at ca. 68 ppm and 184 ppm, respectively. The peak at ca. 14 ppm was attributed to a butyl group connected tin atom. All these signals indicated that another block exists. In addition, the carbonyl group absorption of acid at 1703 cm^{-1} completely disappeared in the IR spectra (Fig. 7), which also demonstrated the reaction

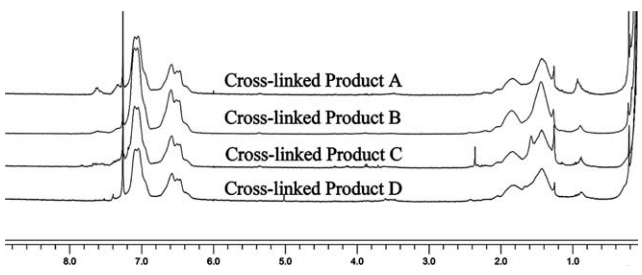

Figure 5 ^{1}H-NMR spectra of the products between **PSt-*b*-PVPHA** and *n*-Bu_2SnO, crosslinked product **A**: product between **PSt$_{203}$-*b*-PVPHA$_{13}$** and *n*-Bu_2SnO, crosslinked product **B**: product between **PSt$_{196}$-*b*-PVPHA$_{34}$** and *n*-Bu_2SnO, crosslinked product **C**: product between **PSt$_{196}$-*b*-PVPHA$_{51}$** and *n*-Bu_2SnO, crosslinked product **D**: product between **PSt$_{196}$-*b*-PVPHA$_{103}$** and *n*-Bu_2SnO.

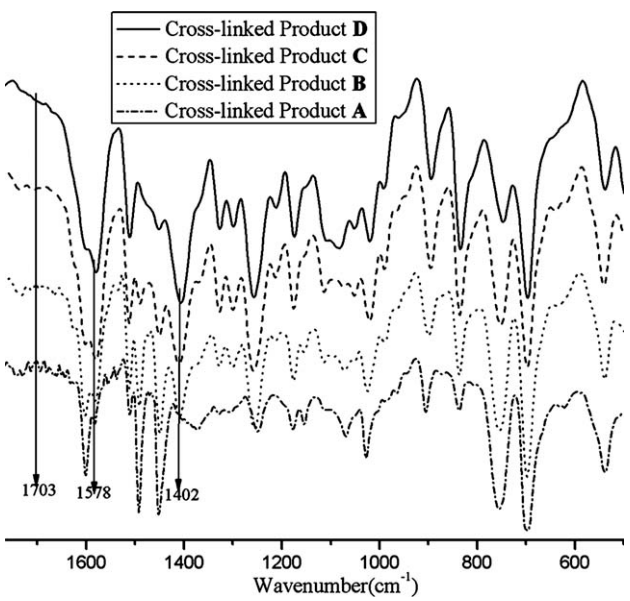

Figure 7 FTIR spectra of crosslinked product **A**, B, C, and D.

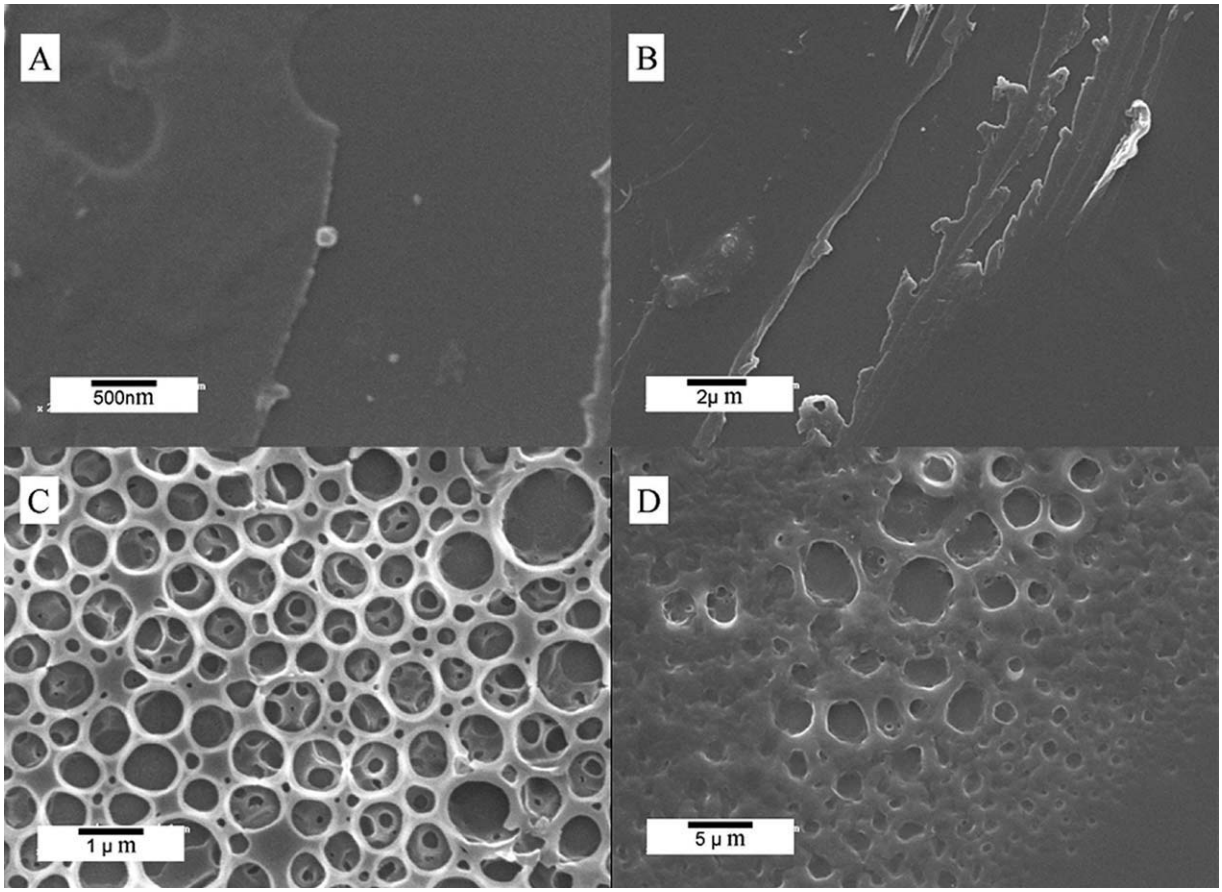

Figure 8 SEM images of PSt-*b*-PVPHA in THF, (A) PSt_{203}-*b*-$PVPHA_{13}$, (B) PSt_{196}-*b*-$PVPHA_{34}$, (C) PSt_{196}-*b*-$PVPHA_{51}$, and (D) PSt_{196}-*b*-$PVPHA_{103}$.

between the *n*-Bu_2SnO and **VPHA** units was complete. Furthermore, two new absorption signals (1578 cm^{-1} and 1402 cm^{-1}) were assigned to the antisymmetrical stretching vibration of the —C(O)O— group and the symmetrical stretching vibration of the —C(O)O— group, respectively. The difference between the two vibration frequencies ($v = v_{as} - v_s$) was $\sim$ 176 cm^{-1}, indicating the existence of both monodentate coordination and bidentate coordination modes of the —C(O)O— group to the tin atom in the resulting copolymers.[44] The crosslinking degree is a very important parameter for the crosslinking of polymer. In this study, the ratio of —COOH groups to *n*-Bu_2SnO was set at 2 : 1, which promoted the production of diorganotin carboxylate. The carbonyl absorption of —COOH group of **PSt-*b*-PVPHA** at 1703 cm^{-1} completely disappeared compared with the IR spectra of crosslinked product, which indicated almost all the —COOH groups reacted with *n*-Bu_2SnO. In Figure 6, C=O carbon just showed one sharp peak in the ^{13}C-NMR, corresponding to the diorganotin carboxylate C=O carbon, which also excluded the presence of —COOH groups. As shown above, it was concluded that almost all the —COOH groups involved in the crosslinking reaction.

Morphology study

As far as amphiphilic diblock copolymers are concerned, one of the most interesting properties is their ability to self-assemble into a large variety of structures. In general, a given polymer's morphologies may change with temperature, copolymer composition, volume fraction, molecular weight of the copolymer, and occasionally with concentration.[45–48] Thus, to investigate the effect of polymer molecular weight on the morphology, all external factors herein were maintained constant except for the change of polymer molecular weight. The morphologies of **PSt-*b*-PVPHA** were studied by SEM. SEM images showed (Fig. 8) that the **PSt_{203}-*b*-$PVPHA_{13}$** and **PSt_{196}-*b*-$PVPHA_{34}$** were dispersed as film-like on the glass substrates. And the copolymers **PSt_{196}-*b*-$PVPHA_{51}$** and **PSt_{196}-*b*-$PVPHA_{103}$** showed the honeycomb patterns. The formation of honeycomb structure is related to the water content. The higher water content could condense onto the solution surface leading to coalescence of water droplets resulting in larger pore size.[49,50] In view of the formation of honeycomb structure, we proposed the mechanism of morphology for the **PSt-*b*-PVPHA** (Fig. 9). The **PSt_{196}-*b*-$PVPHA_{51}$** and **PSt_{196}-*b*-$PVPHA_{103}$** with

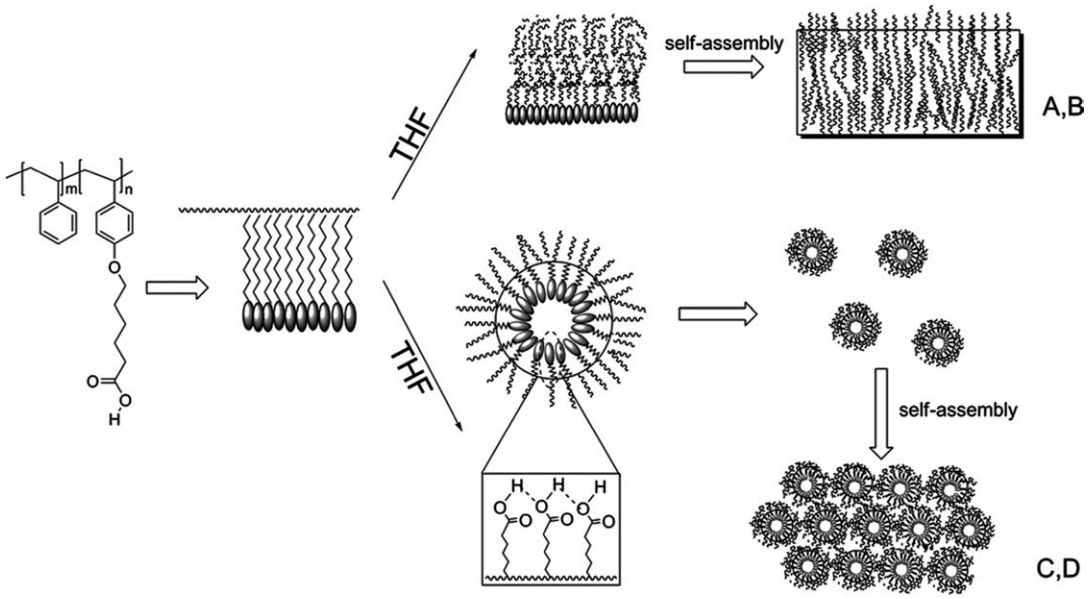

Figure 9 The proposed formation mechanism of PSt-*b*-PVPHA's morphologies, (A) PSt_{203}-*b*-$PVPHA_{13}$, (B) PSt_{196}-*b*-$PVPHA_{34}$, (C) PSt_{196}-*b*-$PVPHA_{51}$, and (D) PSt_{196}-*b*-$PVPHA_{103}$.

the longer **PVPHA** segments resulted in a structure with the **PVPHA** pointing inward away from the solvent outside in THF. It is because the THF is a good solvent for the **PSt**, whereas it is a poor solvent for the **PVPHA**. In addition, due to the longer **PVPHA** segments with the stronger hydrogen-bond effect and further absorbing more water molecules, the **PSt_{196}-*b*-$PVPHA_{103}$** showed a larger pore size

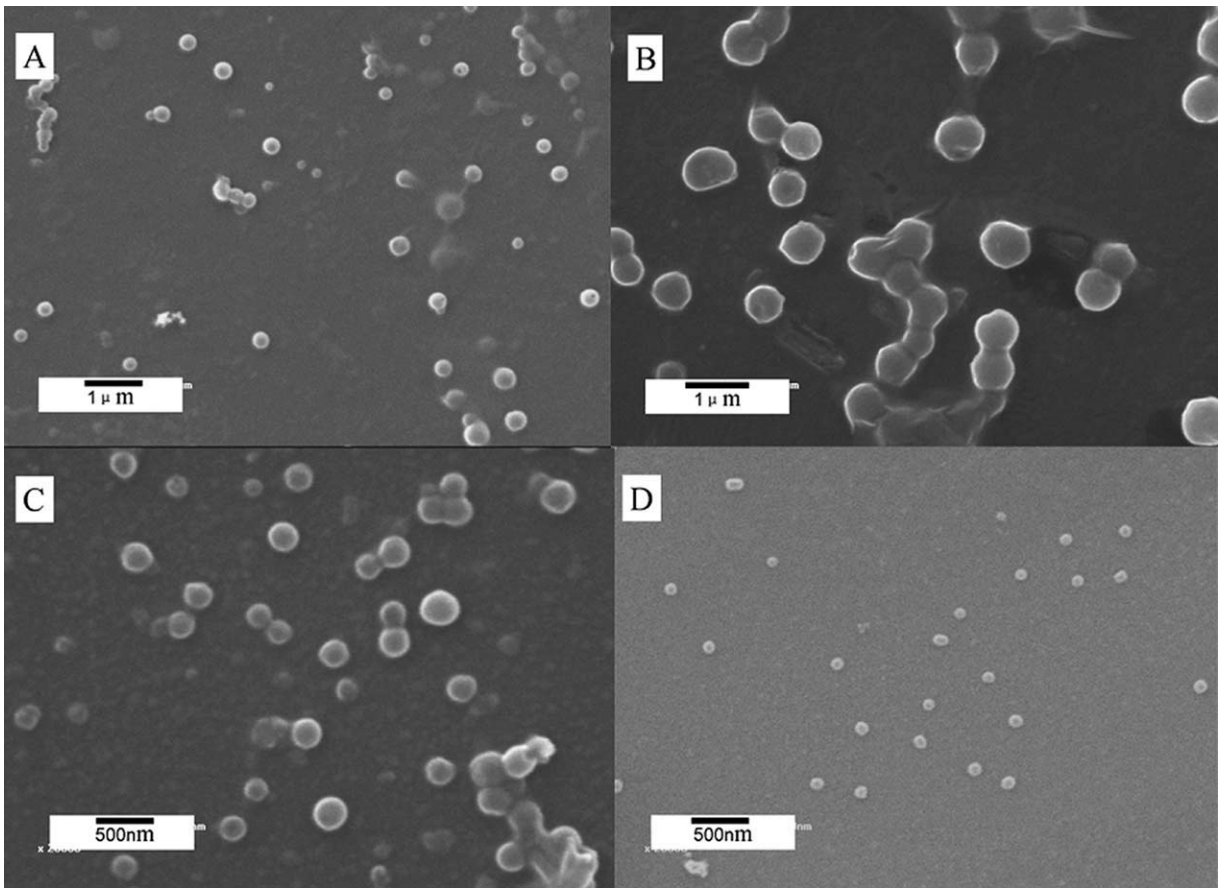

Figure 10 SEM images of crosslinked product **A**, B, C, and D.

TABLE II
The Diameters of Crosslinked Products Between PSt-*b*-PVPHA and *n*-Bu_2SnO

Crosslinked product[a]	$Diameter_{SEM}$[b] (nm)	$Diameter_{DLS}$[c] (nm)
A	300/150	10/80
B	680	910
C	260	320
D	90	190

[a] **A:** Crosslinked product between $\mathbf{PSt_{203}}$-*b*-$\mathbf{PVPHA_{13}}$ and *n*-Bu_2SnO, **B:** crosslinked product between $\mathbf{PSt_{196}}$-*b*-$\mathbf{PVPHA_{34}}$ and *n*-Bu_2SnO, **C:** crosslinked product between $\mathbf{PSt_{196}}$-*b*-$\mathbf{PVPHA_{51}}$ and *n*-Bu_2SnO, **D:** crosslinked product between $\mathbf{PSt_{196}}$-*b*-$\mathbf{PVPHA_{103}}$ and *n*-Bu_2SnO.
[b] Determined by SEM.
[c] Determined by DLS.

than that of $\mathbf{PSt_{196}}$-*b*-$\mathbf{PVPHA_{51}}$. However, the P$\mathbf{St_{203}}$-*b*-$\mathbf{PVPHA_{13}}$ and $\mathbf{PSt_{196}}$-*b*-$\mathbf{PVPHA_{34}}$ with the shorter **PVPHA** segments just showed film-like on the glass substrates. This may be just the result of phase separation because the weaker hydrogen-bond effect cannot absorb water molecule.

As for the morphologies of the different crosslinked products, SEM analysis were also applied (Fig. 10). In the previous reports, the triorganotin-containing polymers did not display any self-assembly ability.[28] Nevertheless, herein the dibutyltin-containing crosslinked products possessed the versatile self-assembly properties based on the strong interaction between Sn and O. It could be found that these dibutyltin-containing crosslinked products self-assembled into micelles in THF and were well dispersed as individual nanoparticles with regularly spherical shape in SEM images. And the diameters of individual nanoparticles were different (Table II). As to crosslinked product **A**, the interaction of interpolymer chain was relatively weak since the shortest organotin carboxylate segment showed the lower extent of crosslinking.

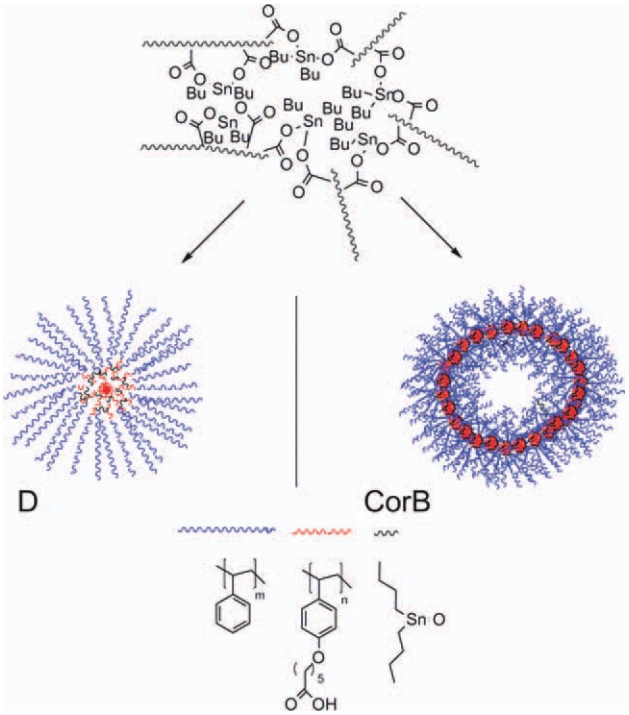

Figure 11 The proposed formation mechanism of organotin-containing core-shell nanoparticles. [Color figure can be viewed in the online issue, which is available at wileyonlinelibrary.com.]

Thereby, the sizes of crosslinked product **A** were versatile (from 150 to 300 nm). From crosslinked product **B** to **C** to **D**, the diameters in SEM decreased gradually with increasing organotin carboxylate segment, from 680 nm to 260 nm to 90 nm, respectively. At the meantime, DLS measurements gave a similar change trend of hydrodynamic diameters that were in agreement with the SEM diameters (Table II). According to DLS analysis, diameters were all larger than the ones measured by SEM, which can be due to the collapse during the drying process (Supporting Information

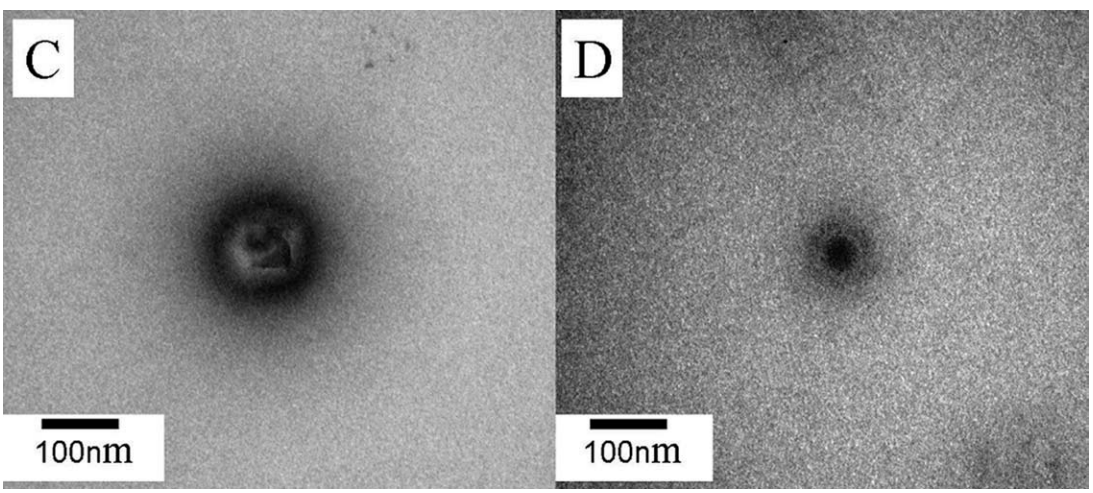

Figure 12 TEM images of crosslinked product C and D.

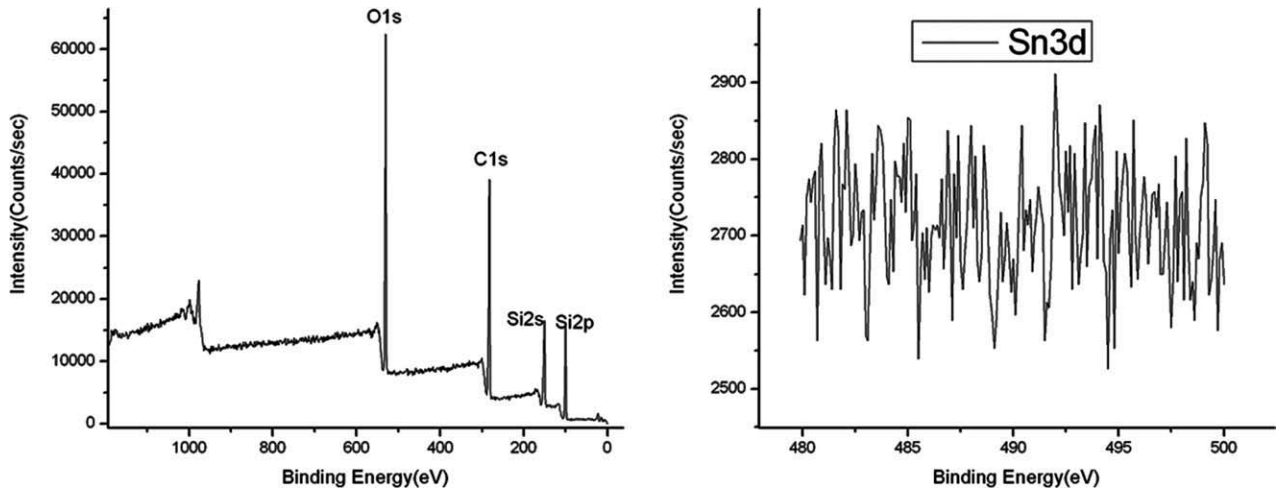

Figure 13 XPS spectra of crosslinked product D.

Fig. S3).[27] In addition, the diameters from SEM of crosslinked product **B** (680 nm) and **C** (260 nm) were both larger than their estimated diameters, $247 \times 2 \times 0.25 = 124$ nm and $230 \times 2 \times 0.25 = 115$ nm, respectively. Conversely, the diameter of crosslinked product **D** (90 nm) was smaller than the estimated diameter, $299 \times 2 \times 0.25 = 150$ nm.[51] This kind of unusual phenomenon may be explained by the formation of the hollow core structure (crosslinked products **B** and **C**) and solid spherical nanoparticles (crosslinked product **D**). In details, in the case of crosslinked product **D**, the longest organotin carboxylate segment led to the enhancement of crosslinking extent, which may induce the formation of solid spherical nanoparticles containing an organotin carboxylate core and a polystyrene shell (Fig. 11). This is also consistent with the disappearance of NMR signals from organotin carboxylate. Whereas as to crosslinked product **B** and **C**, the larger solid spherical nanoparticles could not be formed through the further aggregation of preformed smaller solid spherical nanoparticles containing an organotin core and a polystyrene shell, because there was no strong interaction between the polystyrene shell layer. Furthermore, the above explanation was also supported by TEM. TEM images clearly showed the presence of tin atoms in the core of the nanoparticle for the crosslinked product **D** (Fig. 12). The hollow core structure was also found in the TEM image of crosslinked product **C**. Nevertheless, the measured diameters were slightly larger than that from SEM images. In any event, the diameters in SEM decreased with increasing organotin carboxylate length.

XPS was also performed to probe the elemental composition of the nanoparticles on the surface. As seen in the spectra (Fig. 13), only peaks for carbon, oxygen, and silicon were visible. The Si and O peaks were representative of the glass substrate and the C peak was assigned to polystyrene. The wide-scan XPS and high resolution XPS did not show Sn peak yet. This data demonstrated that only polystyrene was on the surface of nanoparticles, and the organotin carboxylate was completely surrounded by polystyrene. These organotin-containing core-shell nanoparticles, likely microreactor, may be a good model for catalysis.

CONCLUSIONS

A series of novel well-defined organic/inorganic hybrid nanoparticles bearing an organotin core and a polystyrene shell were prepared by the crosslinking of **VPHA** units with *n*-Bu_2SnO. The morphologies of nanoparticles, including hollow core and solid spherical nanoparticles, were investigated by the TEM, SEM, and XPS study. The results showed that the length of **VPHA** units plays an important role on formation of the morphologies and the size of micelle. Moreover, the mechanism of the morphological transformation was surmised, and it will be helpful for the following studies of organotin-containing polymers. And it is the key that these kinds of morphologies may be good catalysts for esterification and transesterification reactions, because of their cluster-like structures of organotin. Thus, the future work will focus on the applications of these nanoparticles as catalysts of esterification and transesterification reactions.

The authors thank Professor Pingchuan Sun, Dr. Xingdi Zhou, Yuping Liu, and Huijing Zhou (all of Nankai University, China) for their help with the solid-state NMR, TEM, XPS, and SEM measurements, respectively.

References

1. Hawker, C. J.; Wooley, K. L. Science 2005, 309, 1200.
2. Bates, F. S.; Fredrickson, G. H. Annu Rev Phys Chem 1990, 41, 525.
3. Massey, J. A.; Winnik, M. A.; Manners, I.; Chan, V. Z.-H.; Ostermann, J. M.; Enchelmaier, R.; Spatz, J. P.; Möller, M. J Am Chem Soc 2001, 123, 3147.

4. Yan, X. H.; Liu, G. J.; Li, Z. J Am Chem Soc 2004, 126, 10059.
5. Silva, G. A.; Czeisler, C.; Niece, K. L.; Beniash, E.; Harrington, D. A.; Kessler, J. A.; Stupp, S. I. Science 2004, 303, 1352.
6. Kataoka, K.; Harada, A.; Nagasaki, Y.; Adv Drug Delivery Rev 2001, 47, 113.
7. Savic, R.; Luo, L. B.; Eisenberg, A.; Maysinger, D. Science 2003, 300, 615.
8. Moad, G.; Rizzardo, E.; Thang, S. H. Aust J Chem 2005, 58, 379.
9. Kamigaito, M.; Ando, T.; Sawamoto, M. Chem Rev 2001, 101, 3689.
10. Sciannamea, V.; Jerome, R.; Detrembleur, C. Chem Rev 2008, 108, 1104.
11. Matyjaszewski, K.; Xia, J. H. Chem Rev 2001, 101, 2921.
12. Whittell, G. R.; Manners, I. Adv Mater 2007, 19, 343934.
13. Williams, K. A.; Boydston, A. J.; Bielawski, C. W. Chem Soc Rev 2007, 36, 729.
14. Manners, I. Angew Chem Int Ed Engl 1996, 35, 1602.
15. Manners, I. Science 2001, 294, 1664.
16. Manners, I. Synthetic Metal-Containing Polymers, Chapter 5; Wiley-VCH: Weinheim, 2004.
17. Du, J.; Chen, Y. Macromolecules 2004, 37, 5710.
18. Du, J., Chen, Y. Macromolecules 2004, 37, 6322.
19. Du, J.; Chen, Y. Angew Chem Int Ed Engl 2004, 43, 5084.
20. Zhang, K.; Yu, X.; Gao, L.; Chen, Y.; Yang, Z. Langmuir 2008, 24, 6542.
21. Angiolini, L.; Caretti, D.; Salatelli, E.; Mazzocchetti, L.; Willem, R.; Biesemans, M. J Inorg Organomet Polym 2008, 18, 236.
22. Angiolini, L.; Caretti, D.; Mazzocchetti, L.; Salatelli, E.; Willem, R.; Biesemans, M. J Polym Sci Part A: Polym Chem 2005, 43, 3091.
23. Angiolini, L.; Caretti, D.; Mazzocchetti, L.; Salatelli, E.; Willem, R.; Biesemans, M. J Organomet Chem 2006, 691, 3043.
24. Angiolini, L.; Caretti, D.; Mazzocchetti, L.; Salatelli, E.; Willem, R.; Biesemans, M. Appl Organomet Chem 2005, 19, 841.
25. Pinoie, V.; Biesemans, M.; Willem, R. Organometallics 2010, 29, 193.
26. Pinoie, V.; Biesemans, M.; Willem, R. Appl Organomet Chem 2010, 24, 135.
27. Xu, Z.; Yin, S.; Lei, B.; Lu, Y.; Chang, W.; Li, J. J Polym Sci Part A: Polym Chem 2007, 45, 942.
28. Feng, G.; Jia, Y.; Liu, L.; Chang, W.; Li, J. J Polym Sci Part A: Polym Chem 2010, 48, 5992.
29. Lei, B.; Jian, J.; Jia, Y.; Liu, L.; Chang, W.; Li, J. J Organomet Chem 2011, 696, 1416.
30. Chemin, A.; Deleuze, H.; Maillard, B. J Appl Polym Sci 2001, 79, 1297.
31. Ingham, R. K.; Rosenberg, S. D.; Gilman, H. Chem Rev 1960, 60, 459.
32. Pellerito, L.; Nagy, L. Coord Chem Rev 2002, 224, 111.
33. García-Zarracino, R.; Höpfl, H. Angew Chem Int Ed Engl 2004, 43, 1507.
34. García-Zarracino, R.; Höpfl, H. J Am Chem Soc 2005, 127, 3120.
35. Holmes, R. R. Acc Chem Res 1989, 22, 190.
36. Dharia, J. R.; Pathak, C. P.; Babu, G. N.; Gupta, S. K. J Polym Sci Part A: Polym Chem 1988, 26, 595.
37. Liu, J.; Shang, H.; Zheng, Y.; Song, X. J Appl Polym Sci 2009, 113, 1216.
38. Gielen, M. Chim Nouv 2001, 76, 3333.
39. Tsagatakis, J. K.; Chaniotakis, N. A.; Jurkschat, K.; Damoun, S.; Geerlings, P.; Bouhdid, A. Helv Chim Acta 1999, 82, 531.
40. Otera, J. Chem Rev 1991, 93, 1449.
41. Vosloo, J. J.; De Wet-Roos, D.; Tonge, M. P.; Sanderson, R. D. Macromolecules 2002, 35, 4894.
42. Cammidge, A. N.; Downing, S.; Ngaini, Z. Tetrahedron Lett 2003, 44, 6633.
43. Epple, R.; Kudirka, R.; Greenberg, W. A. J Comb Chem 2003, 5, 292.
44. Szorcsik, A.; Nagy, L.; Gajda-Schrantz, K.; Pellerito, L.; Nagy, E.; Edelmann, F. T. J Radioanal Nucl Chem 2002, 252, 523.
45. Yoshida, T.; Tarigabil, R.; Hillmyer, M. A.; Lodge, T. P. Macromolecules 2007, 40, 1615.
46. Discher, D. E.; Eisenberg, A. Science 2002, 297, 967.
47. Zhang, L.; Eisenberg, A. Science 1995, 268, 1728.
48. Fenouillot, F.; Cassagnau, P.; Majesté, J. C. Polymer 2009, 50, 1333.
49. Deepak, V. D.; Asha, S. K. J Polym Sci Part A: Polym Chem 2008, 46, 1278.
50. Deepak, V. D.; Asha, S. K. J Phys Chem B 2006, 110, 21450.
51. Babin, J.; Lepage, M.; Zhao, Y. Macromolecules 2008, 41, 1246.